



Development of Ti-Zr-Mn based AB₂ type metal hydrides alloys for an 865 bar two-stage hydrogen compressor

Rui Li^{a,b,c,*}, Akhil Penmathsa^{a,b,c}, Tai Sun^c, Noris Gallandat^c, Jinyu Li^d, Jihye Park^e, Han-Jin Kim^e, Pyungsoon Kim^e, Narae Yoon^e, Ji-Hoon Jang^e, Andreas Züttel^{a,b}

^a Laboratory of Materials for Renewable Energy (LMER), Institute of Chemical Sciences and Engineering (ISIC), École Polytechnique Fédérale de Lausanne, EPFL Valais/Wallis, 1950, Sion, Switzerland

^b Empa Materials Science and Technology, 8600, Dübendorf, Switzerland

^c GRZ Technologies Ltd, CH-1580, Avenches, Switzerland

^d XTC Hydrogen Energy Science and Technology (Xiamen) Ltd., Xiamen, 361004, China

^e Hyundai Motor Company, 37, Cheoldobangmulgwan-ro, Uiwang-si, Gyeonggi-do, 16082, South Korea

ARTICLE INFO

Keywords:

Metal hydrides
Hydrogen compressor
Hydrogen compression
Hydrogen storage
Cycle stability
Hydrogen refueling station

ABSTRACT

This study reports the development of a new Ti-Zr-Mn-based AB₂ type hydrogen storage alloys for a two-stage metal hydride hydrogen compressor (MHHC). The hydrogen storage alloys are designed to compress hydrogen from 35 to 865 bar within a temperature difference of 115 °C. High-pressure PCT measurements up to 700 bar were carried out to test the performance of the alloys. The alloys' hysteresis and the plateau slope were reduced by optimizing the composition. The introduction of fugacity correction into the Van't Hoff equation reduces the deviation between calculation and actual pressure to 24 bar at a pressure above 350 bar. A precise relation between the Ti/Zr ratio and the desorption pressure is described and helps make a correct design of the alloy composition. The designed alloy shows losses less than 1% of the capacity over 3000 full cycles. The desorption plateau pressure of the alloy is constant within 92% during the whole cycling process. A 2 stages compressor working with two types of alloys offers compression with a temperature range between -20 and 95 °C for the refueling hydrogen vehicles up to 865 bar.

1. Introduction

Hydrogen is a green and non-polluting energy vector with high energy density and is considered one of the most promising new-generation fuels [1]. Significant progress has been made in the preparation, storage, transportation, and utilization of hydrogen [2,3]. Fuel cell electric vehicles (FCEV) are a major field of hydrogen applications [4,5]. FCEV mainly adopt high-pressure hydrogen storage cylinders to ensure a sufficient driving range at a comparatively high gravimetric density [6]. Therefore, developing hydrogen compressors with high safety, high output pressures, and high efficiency is one of the most important targets for the construction of hydrogen refueling stations.

MHHC, a compression method brimming with potential, stands out when compared to traditional mechanical hydrogen compressors [7]. Thermally-driven MHHC avoids the problems of noise and high maintenance cost, as it operates without any moving parts in the whole

system [8]. Industrial waste heat can serve as an effective energy source to drive MHHC, enabling the continuous and stable production of high-purity hydrogen. MHHC can be designed to be compact, making them suitable for applications where space is limited, such as in densely populated urban areas. This makes them ideal for applications such as hydrogen refueling stations. MHHC have a wide range of applications beyond hydrogen fueling stations, such as the integration in various industrial processes. Their versatility makes them an important piece of the puzzle contributing to the widespread adoption of hydrogen as a clean energy carrier.

The concept of MHHC was initially proposed 50 years ago. Reilly et al. reported on a hydrogen compressor that used vanadium-based hydride to absorb hydrogen at 18 °C and release high-pressure hydrogen at 24 atm after heating to 50 °C [9]. In many cases, a single-stage compression relying on a single type of material within a limited operating temperature range is not sufficient for achieving the

* Corresponding author. Laboratory of Materials for Renewable Energy (LMER), Institute of Chemical Sciences and Engineering (ISIC), École Polytechnique Fédérale de Lausanne, EPFL Valais/Wallis, 1950, Sion, Switzerland.

E-mail address: rui.li@epfl.ch (R. Li).

<https://doi.org/10.1016/j.ijhydene.2024.05.336>

Received 6 March 2024; Received in revised form 13 May 2024; Accepted 21 May 2024

0360-3199/© 2024 Hydrogen Energy Publications LLC. Published by Elsevier Ltd. All rights are reserved, including those for text and data mining, AI training, and similar technologies.

desired delivery pressure. Therefore, a multi-stage design is necessary [10] when the compression ratio is larger than 15 in a temperature range of $\Delta T < 115$ °C. The operating temperature range usually depends on the temperature of heating and cooling sources, such as industrial steam (120–140 °C) and cooling water (15–25 °C) [11]. Minimizing the number of hydrogen compressor stages is critical to enhance the overall MHHC efficiency under given operating conditions. As a result, the composition of hydrogen storage alloys used in MHHC must be carefully optimized to maximize the released hydrogen pressure and hydrogen storage capacity at each stage. At the same time, the hydrogen absorption plateau pressure at the next stage should be matched to the hydrogen desorption plateau pressure at previous stage [12]. The hydrogen storage alloys suitable for MHHC should [8] have a low plateau slope, low hysteresis, high hydrogen storage capacity, good absorption and desorption kinetics properties, low production cost, and excellent cycle stability. Furthermore, alloy design necessitates careful consideration of activation performance and the ability to finely tune the plateau pressure for optimal performance.

AB₅-type metal hydride alloys exhibit fast kinetics and easy activation [13]. However, their application is hindered by high production cost and poor cycle stability [14]. In contrast, AB-type TiFe-based metal hydride alloys have higher hydrogen storage capacity at room temperature and lower raw material cost. However, they are difficult to activate, and the range of adjustment for the plateau pressure is limited [15]. A second plateau is prone to appear during the hydrogen absorption and desorption process. These disadvantages also limit the practical application of TiFe-based alloys [16] in the hydrogen compression field. AB₂ metal hydride alloys have a high hydrogen storage capacity, good hydrogen absorption and desorption kinetics, and excellent activation performance. Among various AB₂ metal hydride alloys, TiCr₂-based metal hydride alloys show more potential in hydrogen compression, due to their ability to achieve a broad adjustment range for hydrogen absorption and desorption plateau pressure with high hydrogen storage capacity [17]. However, TiCr₂-based metal hydride alloys still face the challenge of a high plateau slope and low useful capacity. Non-stoichiometric ratios and alloying can change the alloy's unit cell volume, bulk modulus, electron concentration, enthalpy, and entropy. This could help tune the alloy's plateau properties [18].

The tuning the composition of AB₂ alloys has been proved to be an efficient method to optimize the hydrogen storage performance. Indeed, Ti and Zr are the hydride-forming elements on A side. Choice of elements and composition on B side (Fe, Co, Ni, Mn, Al, Cr and V) can achieve the high catalytic activity facilitating splitting of the molecular hydrogen and improve the surface activity of hydrogen exchange with the optimal ratio of mixing. AB₂ type alloys, based on C14 Laves phase intermetallic, can be able to compress hydrogen gas to extremely high pressure (above 1000 bar H₂) while utilizing moderate heating up to 150–170 °C [19]. Ti-Cr-Mn-based or Ti-Cr-Fe-based metal hydride alloys are often used in high-pressure MHHC systems because of their very high hydrogen desorption plateau pressure, low raw material cost, and wide adjustable range of the plateau. In 1999, Vanhannen [20] used the TiCrMn_{0.55}Fe_{0.3}V_{0.15} alloy in the MHHC system for the first time, and compressed hydrogen from 80 bar to nearly 200 bar in a temperature range of 20–60 °C. Corgnale et al. [21] designed a two-stage MHHC with a compression ratio of 4.5, in which Ti_{1.1}CrMn is used as the second-stage material. The second stage alloy can absorb hydrogen under 100 bar at 40 °C and release 450 bar hydrogen at 140 °C. The hydrogen compressor designed by Wang et al. uses (Ti_{0.97}Zr_{0.03})_{1.1}Cr_{1.6}Mn_{0.4} alloy, which shows small hysteresis and good activation performance. This alloy can compress hydrogen from 7 MPa to 45 MPa at 100 °C [22]. Li et al. [23] analyzed the Ti-Zr-Cr-Fe-based alloys and their calculation showed that (Ti_{0.85}Zr_{0.15})_{1.05}Cr_{1.1}Fe_{0.9} alloy can absorb hydrogen at 25 °C under the pressure of 160 bar, then release 455 bar hydrogen at 90 °C. The Ti_{0.8}Zr_{0.2}Cr_{0.95}Fe_{0.95}V_{0.1} alloy designed by Li et al. can theoretically absorb hydrogen at 89 bar at 25 °C and release hydrogen at 845 bar at 150 °C [24]. The alloy

TiCr_{1.55}Mn_{0.2}Fe_{0.2} used in the two-stages MHHC, designed by Guo et al. absorbed hydrogen under the pressure of 71 bar hydrogen at 20 °C and released the pressure of hydrogen more than 1000 bar (theoretical calculation) at 157 °C [25]. The as-cast Ti_{1.08}Cr_{1.3}Mn_{0.2}Fe_{0.5} alloy reported by Peng et al. compress hydrogen from 14 MPa to 89 MPa in a temperature range between 25 °C and 90 °C [26].

This study reports the development of two AB₂-type hydrogen storage alloys to compress hydrogen from 35 bar to 865 bar in a two-stage MHHC. Previous research has shown that Ti-Cr-Mn-Fe alloys are well-suited for high-pressure hydrogen compression [25,26]. Further, Ti-Zr-Cr-Mn alloys have minimal hysteresis and excellent activation performance [22]. Therefore, the Ti-Zr-Cr-Mn-Fe series alloys should have significant potential in hydrogen compression applications. This study introduces a rapid method to design alloy by investigating the correlation between the molar ratio of two elements in alloy compositions and hydrogen storage performance. Additionally, this study offers an improved calculation method for precisely estimating the high desorption pressure, facilitating a relative accurate evaluation of the relationship between critical composition and hydrogen desorption performance.

2. Experimental procedures

2.1. Alloy preparation

Ti, Zr, Cr, Co, Al, Fe and Mn with a purity higher than 99.9% were used as raw materials for the synthesis. The Ti_xZr_y(Cr, Co, Al)_{1.1}Mn_cFe_d ($x = \frac{a}{b} = 4.00, 4.88, 6.14$; $y = \frac{c}{d} = 0.29, 0.52, 0.83, 13.28, 19.00$, molar ratio) alloys were synthesized by induction melting under an Ar atmosphere. The as-prepared hydrogen storage alloys were in the shape of flakes. Considering the loss of Mn during the melting, an additional 5 wt % Mn was added to ensure the accuracy of the composition. The as-prepared flake-like alloys were crushed into fine particles of 1 mm and used for morphology and phase analysis and hydrogen storage performance testing. The alloy for structural analysis was ground to less than 300 mesh.

2.2. Structural analysis

The phase and crystal structures of the samples were investigated by X-ray powder diffraction (Bruker Advance D8) with Cu K_α radiation operating at 40 kV and 40 mA. The scan step is 0.02°/s, and the 2θ range is 20–90°. The lattice parameters are calculated from the XRD pattern using the hexagonal C14-Laves phase structure model.

2.3. Hydrogen storage performance analysis

The hydrogen absorption and desorption isotherms of the samples was measured by the GRZ custom-made equipment AGAS-C (Sievert-type, max measurement pressure of 200 bar) and the commercial RuboSORP-700 (Gravimetric-type, max measurement pressure of 700 bar) with magnetic levitation scale. The AGAS-C detects the changes of the pressure in the sample and calculates the corresponding hydrogen storage capacity. The RuboSORP-700 detects the real-time weight changes in the sample by a high sensitivity balance and calculates the hydrogen storage capacity. The samples were fully activated by high temperature and high pressure before conducting the PCT measurement. The PCT curves of the samples were measured under different temperatures to analyze the hydrogen storage performance.

The cycle stability test was measured at a constant temperature of –20 °C. The absorption plateau pressure of the sample is 27.2 bar, and when the hydrogen pressure is 35 bar, the sample can be charged over 90%. Although the cycling stability of the metal hydride will decrease under 95 °C, the desorption pressure is 397.3 bar at 95 °C, which is over the limiting maximum pressure of the equipment. Thus, we investigated

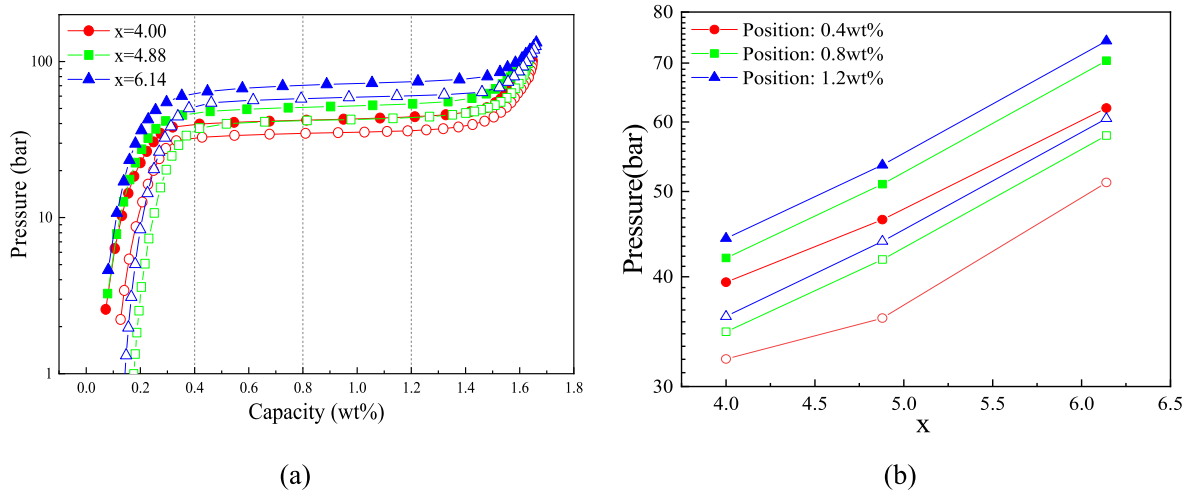


Fig. 1. (a) PC isotherms at $T = 0\text{ }^{\circ}\text{C}$ for absorption (filled markers) and desorption (open markers) measured after activation of the alloys with different Ti/Zr ratios ($x = 4.00, 4.88, 6.14$); (b) Relationship between different Ti/Zr ratio x and absorption (filled markers) and desorption (open markers) plateau pressure at 0.4 wt%, 0.8 wt% and 1.2 wt%.

the cycling performance at constant temperature ($-20\text{ }^{\circ}\text{C}$). The cycling process was that the sample was charged at a constant pressure of 35 bar, then discharged with vacuum pump (the vacuum $< 10\text{ Pa}$ and maintained for 10 min). PCT isotherm measurements were performed at cycles 0, 1000, 2000, and 3000 to investigate the change in hydrogen storage performance of the alloy.

2.4. Materials and methods

The Van't Hoff equation has been used to estimate the hydrogen absorption and desorption plateau pressure of the metal hydrides [8]:

$$\ln \frac{P}{P_0} = \frac{\Delta H}{RT} - \frac{\Delta S}{R} \tag{1}$$

where ΔH^0 is the enthalpy of ab- or desorption at $25\text{ }^{\circ}\text{C}$ and ΔS^0 is the entropy of ab- and desorption at $25\text{ }^{\circ}\text{C}$. However, when the hydrogen pressure exceeds 5 MPa, the difference between ideal gas pressure and fugacity becomes non-negligible. The real hydrogen gas is described by the van der Waals equation. Research conducted by Charbonnier et al [27] demonstrated that the introduction of fugacity instead of

pressure in the Van't Hoff Equation can effectively enhance the accuracy of the calculation of hydrogen pressure.

$$\ln \frac{f}{f_0} = \frac{\Delta H}{RT} - \frac{\Delta S}{R} = \ln \frac{P}{P_0} + \sum_{i=1}^9 a_i \left(\frac{100}{T} \right)^{b_i} \frac{P^{c_i}}{c_i} \tag{2}$$

In Eq (2), the values of f_0 and P_0 are both 1 bar. The values of a_i, b_i, c_i are the constants of the Lemmon equation [28]. f (bar) is the fugacity at temperature T (K). ΔH (kJ/mol H_2) and ΔS (J/Kmol H_2) are the enthalpy and entropy of the reaction.

3. Results and discussion

3.1. The hydrogen storage performance of the alloys

3.1.1. The relationship between the Ti/Zr ratio and the plateau pressure of the alloy

Alloys with varying Ti/Zr ratio x ($x = \frac{a}{b} = 4.00, 4.88, 6.14$) were synthesized. The isotherms of the Zr-substituted AB_2 alloys exhibit a decreasing hydrogen sorption plateau pressure with an increase in the amount of Zr. This trend is correlated with the expansion of lattice

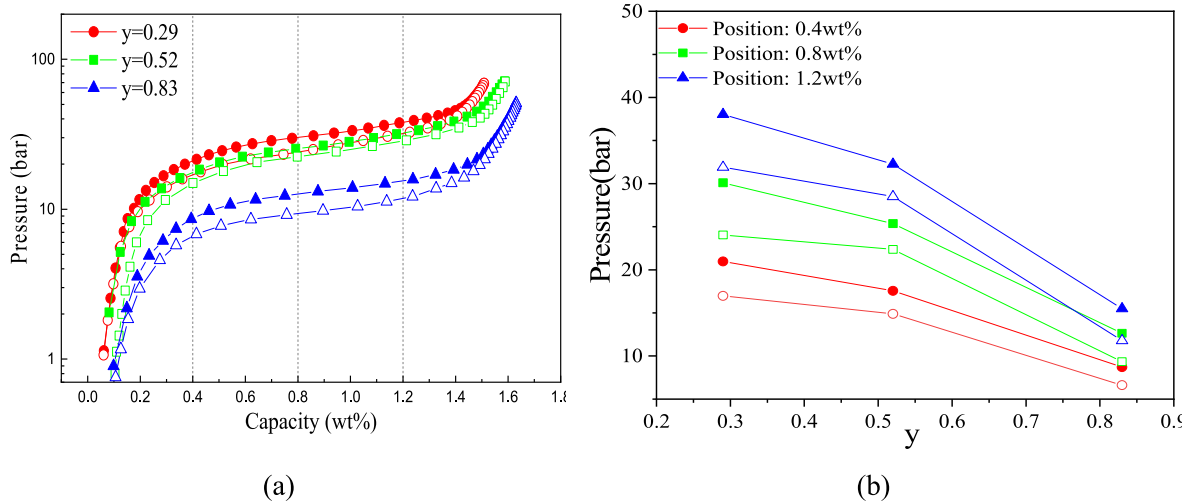


Fig. 2. (a) PC isotherms at $T = 25\text{ }^{\circ}\text{C}$ for absorption (filled markers) and desorption (open markers) measured after activation of the alloys with different Mn/Fe ratios ($y = 0.29, 0.52, 0.83$); (b) Relationship between different Mn/Fe ratio y and absorption (filled markers) and desorption (open markers) plateau pressure at 0.4 wt%, 0.8 wt% and 1.2 wt%.

Table 1

Hydrogen abs/desorption plateau performance of the alloys with different Mn/Fe ratios ($y = 0.29, 0.52, 0.83$).

y	Absorption slope	Desorption slope	Hysteresis
0.29	0.652	0.803	0.222
0.52	0.492	0.579	0.125
0.83	0.582	0.616	0.302

volume and the higher hydrogen binding energy of Zr [29] compared to Ti. Fig. 1 displays the Pressure-Composition-Temperature (PCT) isotherms of the alloys at 0 °C.

Hydrogen absorption plateau pressure (at 0.8 wt%) of the alloy increased from 41.9 bar to 70.5 bar, and the hydrogen desorption pressure (at 0.8 wt%) increased from 34.5 bar to 57.8 bar as x increased from 4.00 to 6.14. Results indicate that adjusting the ratio of Ti/Zr is an effective means to modify the plateau pressure of the hydrogen absorption and desorption. These results will help set the correct Ti/Zr ratio in the final composition design.

3.1.2. The effect of Mn/Fe ratio on the hydrogen isotherm of the Alloy

To quantify the amount of Mn and Fe on the alloy's hydrogen storage performance, AB₂ alloys with different Mn/Fe ratios ($y = \frac{c}{a} = 0.29, 0.52, 0.83$) were prepared. As shown in Fig. 2, the substitution of Fe by Mn has an obvious influence on the plateau pressure, hysteresis, and slope of the alloy's PCT curve.

The calculation of the plateau slope (S) by selecting the pressures of the intersection points of the tangent line of the solid solution area and plateau area as the starting and ending points of the hydrogen absorption and desorption plateau pressure [10], was shown as Equation (3). The pressure of the plateau at the position of 0.8 wt% capacity is taken as the plateau pressure value, and the hysteresis factor (H_f) is calculated by equation (4).

$$S = \ln \frac{P_{start}}{P_{end}} \quad (3)$$

$$H_f = \ln \frac{P_{abs}}{P_{des}} \quad (4)$$

Table 1 shows the value of hydrogen plateau pressure, calculated plateau slope, and hysteresis factor of the alloys with different Mn/Fe ratios. The Substitution of Fe by Mn first reduced and then increased the slope and hysteresis of both the absorption and desorption plateau of the alloy. A minimum value of both slope and hysteresis was found when $y = 0.52$. The increase in Mn/Fe ratio reduces the absorption plateau

pressure (at 0.8 wt%) of the alloy from 30.16 bar to 12.70 bar and the desorption plateau pressure (at 0.8 wt%) reduced from 24.04 bar to 9.40 bar.

3.2. The structure and morphology of the alloys

The XRD patterns of the alloys is shown in Fig. 3. As can be seen, the main phase of the alloys is the C14 type Laves phase (space group P63/mmc, No.194). The variations in the Ti/Zr and Mn/Fe ratios do not alter the structure of the alloys. Besides, with the decrease in the Ti/Zr ratios, the diffraction peaks shift towards lower angles. This shift corresponds to a lattice expansion in the alloys resulting from the substitution of Zr at the Ti site [26]. Table 2 is the calculation of lattice parameters and unit cell volumes. It can be seen that with the increase in the Mn/Fe ratios, the unit cell volumes of the alloys increased from 166.49 Å³ to 167.93 Å³ while the unit cell lattice constant "a" was increased from 4.8986 Å to 4.9089 Å and c increased from 8.0117 Å to 8.0467 Å. This effect is attributed to the larger atomic radius of the Mn element compared to Fe. When Mn atoms replace part of the sites of Fe atoms, the larger atomic radius of Mn atoms expands the unit cell which enable easier entry of hydrogen atoms into the unit cell lattices. It results in the lower plateau pressure.

3.3. Designing target alloys for the MHHC

Fig. 4 is the calculated absorption plateau pressure (-20 °C) and desorption plateau pressure (95 °C) of the alloys with the different Ti/Zr ratio (x) by the Van't Hoff equation with fugacity correction (Eq. (2)). According to the application scenario of the two-stage MHHC designed in this study, the alloy for the first stage of the MHHC is designed to absorb 35 bar of hydrogen from the electrolyzer directly at -20 °C, then

Table 2

Lattice parameter and unit cell volumes of the alloy: with varying Ti/Zr ratio $x = 4.00, 4.88, 6.14$ and $y = 0.52$; with varying Mn/Fe ratio $y = 0.29, 0.52, 0.83$ and $x = 2.33$.

	Lattice parameters (Å)		c/a	Unit cell volume V (Å ³)
	a	c		
x = 4.00	4.8887	7.9998	1.6364	165.58
x = 4.88	4.8802	7.9866	1.6365	164.72
x = 6.14	4.8754	7.9774	1.6362	164.22
y = 0.29	4.8986	8.0117	1.6355	166.49
y = 0.52	4.9053	8.0315	1.6373	167.36
y = 0.83	4.9089	8.0467	1.6392	167.93

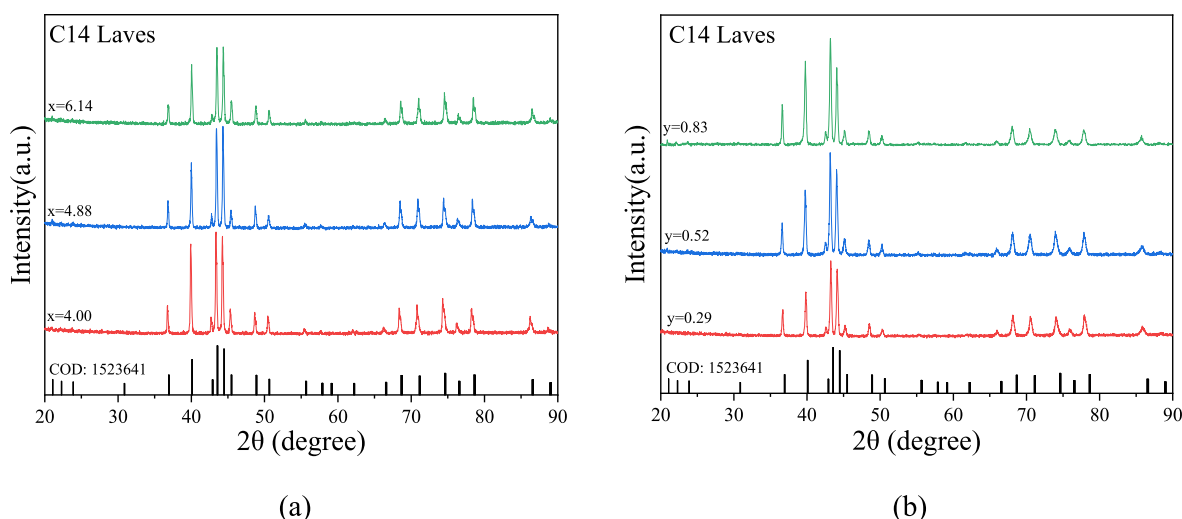


Fig. 3. XRD pattern of the alloys: (a) with varying Ti/Zr ratio $x = 4.00, 4.88, 6.14$; (b) with varying Mn/Fe ratio $y = 0.29, 0.52, 0.83$.

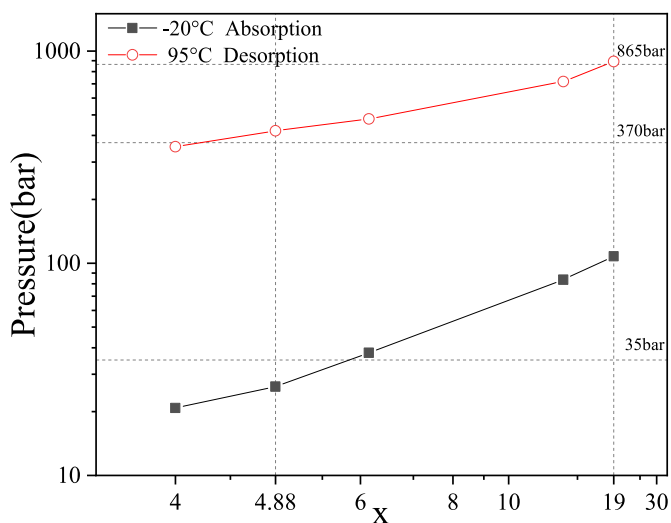


Fig. 4. Relationship between different Ti/Zr ratio x and calculation plateau pressure at absorption temperature ($-20\text{ }^{\circ}\text{C}$) and desorption temperature ($95\text{ }^{\circ}\text{C}$).

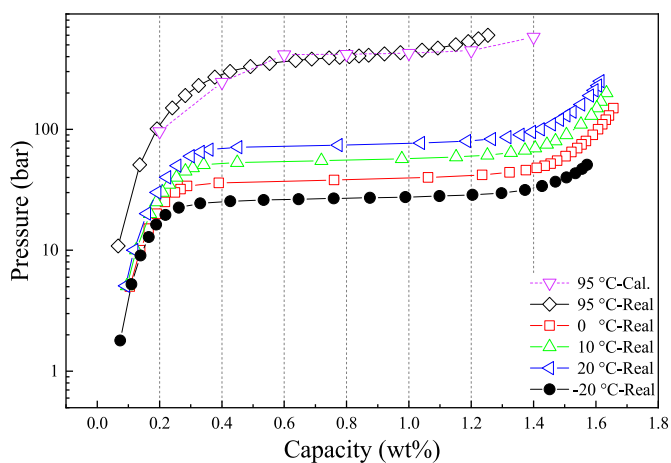


Fig. 5. PC isotherms curves of 1st stage alloy at working temperature $-20\text{ }^{\circ}\text{C}$ and $95\text{ }^{\circ}\text{C}$, and calculated desorption plateau curve at $95\text{ }^{\circ}\text{C}$. (Filled markers: absorption data; Open markers: desorption data).

compress the hydrogen to 370 bar at $95\text{ }^{\circ}\text{C}$. According to the result shown in Fig. 4, when the designed Ti/Zr ratio $x = 4.88$, the alloy can absorb under 35 bar of hydrogen and release hydrogen at a pressure of 421.2 bar at $95\text{ }^{\circ}\text{C}$. The second stage compressor should absorb hydrogen at 370 bar, and then compress the hydrogen to reach 865 bar at $95\text{ }^{\circ}\text{C}$. The result shown in Fig. 4 shows that alloys with varying Ti/Zr ratios can absorb hydrogen from the first stage at $-20\text{ }^{\circ}\text{C}$, but only those alloys with a Ti/Zr ratio higher than 19.00 can release hydrogen at a pressure of 906.2 bar at $95\text{ }^{\circ}\text{C}$.

Two alloys with different Ti/Zr ratios (4.88, 19.00) and optimized B sides were therefore prepared and tested. The PCT curves of the alloy for the first stage ($x = 4.88, y = 0.52$) at designed working temperatures are shown in Fig. 5. The difference in the absorption pressure at $-20\text{ }^{\circ}\text{C}$ between the calculation (26.2 bar, in Fig. 4) and tested pressure (27.2 bar) is very small. Fugacity is a correction to the pressure in an ideal gas, aiming to describe better the behavior of non-ideal systems. This method does not take into account the effect of temperature on enthalpy and entropy of the metal hydride during the compression process. But the results show that the difference in the desorption pressure (at 0.8 wt%) at $95\text{ }^{\circ}\text{C}$ between the calculation (421.2 bar) and tested pressure (397.3 bar) is 23.9 bar. It shows that the calculation result of the plateau

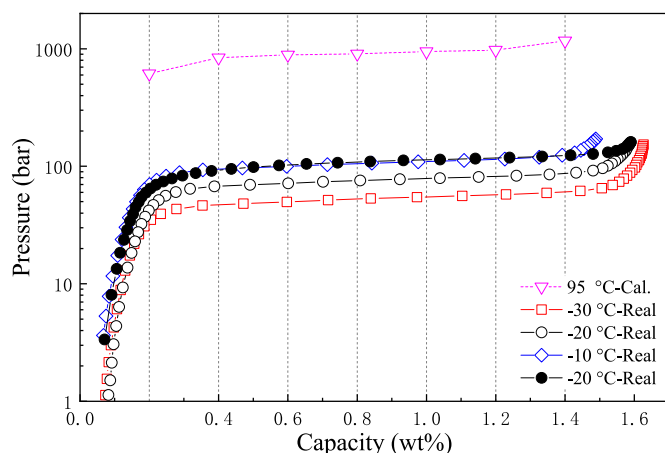


Fig. 6. PC isotherms curves of 2nd stage alloy at working temperature $-20\text{ }^{\circ}\text{C}$ and calculated desorption plateau curve at $95\text{ }^{\circ}\text{C}$. (Filled markers: absorption data; Open markers: desorption data).

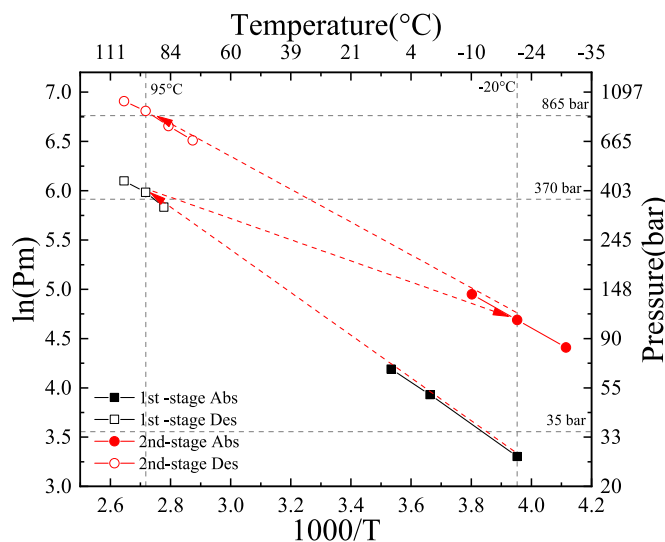


Fig. 7. The compression process of the designed two-stage hydrogen compressor.

pressure is reasonable and close to the actual tested pressure. In terms of the capacity above 1.0 wt% or below 0.5 wt%, it is observed that the tested pressure is higher than the calculated pressure. Thus, the calculated pressure by fugacity correction does not overestimated performance of the metal hydride. Due to the lack of a more precise calculation method, the fugacity corrected calculation is used to approximately demonstrate the performance of the metal hydride. A more precise calculation method is under investigation in detail and will be presented in the next paper.

The PCT curves of the second-stage alloy at designed working temperatures are shown in Fig. 6. As shown in Fig. 6, the hydrogen absorption plateau pressure of the second-stage alloy ($x = 19.00, y = 0.52$) at $-20\text{ }^{\circ}\text{C}$ is 108.8 bar. It is lower than the output pressure of the first-stage alloy at $95\text{ }^{\circ}\text{C}$ and thus has no problem with hydrogen absorption. However, due to the limitation of the device's maximum testing pressure, the PCT curve at $95\text{ }^{\circ}\text{C}$ of the second-stage alloy cannot be directly tested. Therefore, the final performance of the alloy could only be presented by calculation. Through the fugacity correction (Eq. (2) in Section 2.4), the calculation method has been proven to be reasonable and close enough to the actual tested pressure in the first-stage alloy. According to the calculation, the desorption plateau pressure of the

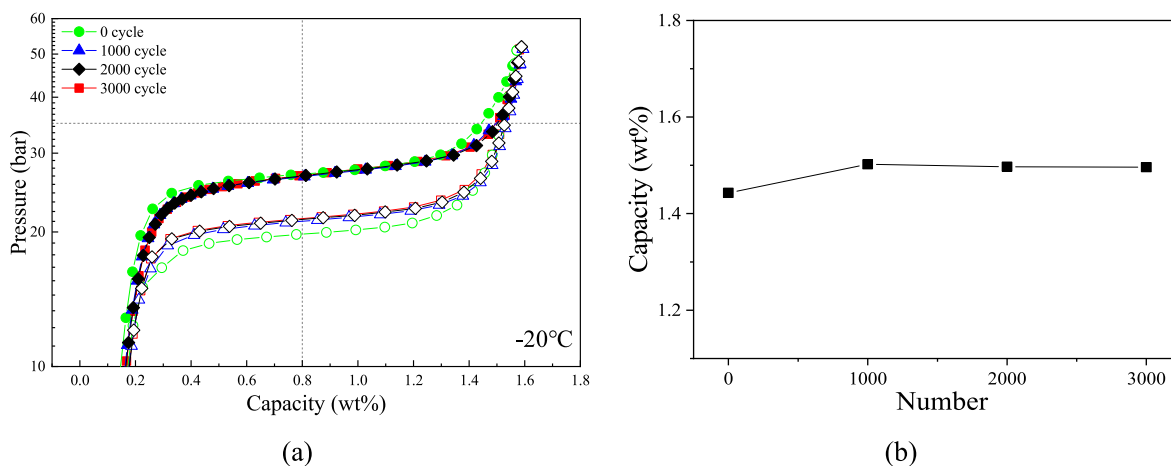


Fig. 8. (a) PC isotherms curves of the first-stage alloy after 0, 1000th, 2000th, and 3000th cycles at $-20\text{ }^{\circ}\text{C}$; (b) the relationship between hydrogen storage capacity and cycling numbers.

second-stage alloy at $95\text{ }^{\circ}\text{C}$ is c.a. 906 bar (at 0.8 wt%) that should be close to the tested plateau pressure. This output pressure fulfills the design target pressure of the second stage MHHC.

Fig. 7 shows the hydrogen compression process of the alloys for the two-stages MHHC. The first-stage alloy absorbs 35 bar of hydrogen at $-20\text{ }^{\circ}\text{C}$ from the electrolyzer. After heating the first-stage alloy to $95\text{ }^{\circ}\text{C}$, hydrogen will be released at 397 bar from the alloy and will be used on medium-pressure hydrogen application or to feed the second-stage alloy at $-20\text{ }^{\circ}\text{C}$. Later on, the second-stage alloy will output hydrogen at a pressure above 865 bar and a temperature of $95\text{ }^{\circ}\text{C}$. This hydrogen could be used to charge the high-pressure hydrogen application.

3.4. Cycling stability analysis

A cyclability test was carried out at $-20\text{ }^{\circ}\text{C}$ to test the stability of the first-stage alloy. Complete PCT measurements were performed at the initial, 1000th, 2000th, and 3000th cycles. As shown in Fig. 8, the initial hydrogen storage capacity of the alloy at 35 bar was 1.45 wt%. After 1000 cycles, the capacity increased slightly to 1.50 wt%. After 2000 cycles, the capacity decreased back to 1.49 wt% and maintained after 3000 cycles. Therefore, it can be concluded that the degradation at 3000 cycles is negligible and within the measurement accuracy. The hydrogen desorption plateau pressure of the alloy increased from 19.70 bar to 21.47 bar after the 1000th cycles, then maintained at c.a. 21 bar after 3000 cycles. The hydrogen absorption plateau pressure is maintained at the range from 26.5 bar to 27 bar during the whole cycling process. This proves that the alloy has excellent cycle stability over a significant number of cycles, and thus is suitable for long-term operation.

4. Conclusions

Ti-Zr-Cr-Mn-Fe alloys as active materials for a two-stage metal hydride hydrogen compressor (MHHC) were developed, which allow the compression of hydrogen from 35 bar to 865 bar, driven by a temperature difference of only $115\text{ }^{\circ}\text{C}$. The plateau pressure of the alloys at high pressure was calculated by the Van't Hoff equation including fugacity correction in order to improve the accuracy of the calculation of the high desorption pressure at high temperature. Two alloys with different Ti/Zr ratios and optimized plateau slope and hysteresis were designed and tested. Results show that the first-stage alloy can absorb 35 bar hydrogen from the electrolyzer and release 397.3 bar hydrogen after heating to $95\text{ }^{\circ}\text{C}$. The second-stage alloy can be fully charged by the first-stage alloy and released hydrogen at a pressure of over 865 bar. A cyclability test demonstrated negligible degradation after 3000 full cycles. The absorption plateau pressure and the storage capacity are both maintained

stable during the cycle tests. This work lays the ground for the design of a high-pressure metal hydrides hydrogen compressor which could be used for the efficient refueling of hydrogen vehicles.

CRediT authorship contribution statement

Rui Li: Writing – review & editing, Writing – original draft, Investigation, Data curation, Conceptualization. **Akhil Penmathsa:** Formal analysis, Data curation. **Tai Sun:** Writing – review & editing, Validation, Supervision, Project administration, Conceptualization. **Noris Gallandat:** Writing – review & editing, Supervision, Project administration, Funding acquisition. **Jinyu Li:** Resources. **Jihye Park:** Writing – review & editing, Validation, Funding acquisition. **Han-Jin Kim:** Writing – review & editing, Funding acquisition. **Pyungsoon Kim:** Writing – review & editing, Validation, Funding acquisition. **Narae Yoon:** Writing – review & editing, Validation, Funding acquisition. **Ji-Hoon Jang:** Writing – review & editing, Supervision, Funding acquisition. **Andreas Züttel:** Writing – review & editing, Validation, Supervision, Funding acquisition.

Declaration of competing interest

The authors declare that they have no known competing financial interests or personal relationships that could have appeared to influence the work reported in this paper.

References

- [1] Züttel A, Gallandat N, Dyson PJ, Schlapbach L, Gilgen PW, Orimo S-I. Future Swiss energy economy: the challenge of storing renewable energy. *Front Energy Res Feb.* 2022;9:785908. <https://doi.org/10.3389/fenrg.2021.785908>.
- [2] Rasul MG, Hazrat MA, Sattar MA, Jahirul MI, Shearer MJ. The future of hydrogen: challenges on production, storage and applications. *Energy Convers Manag Nov.* 2022;272:116326. <https://doi.org/10.1016/j.enconman.2022.116326>.
- [3] Bellosta von Colbe J, et al. Application of hydrides in hydrogen storage and compression: achievements, outlook and perspectives. *Int J Hydrogen Energy Mar.* 2019;44(15):7780–808. <https://doi.org/10.1016/j.ijhydene.2019.01.104>.
- [4] Aminudin MA, Kamarudin SK, Lim BH, Majilan EH, Masdar MS, Shaari N. An overview: current progress on hydrogen fuel cell vehicles. *Int J Hydrogen Energy Feb.* 2023;48(11):4371–88. <https://doi.org/10.1016/j.ijhydene.2022.10.156>.
- [5] Hassan IA, Ramadan HS, Saleh MA, Hissel D. Hydrogen storage technologies for stationary and mobile applications: review, analysis and perspectives. *Renew Sustain Energy Rev Oct.* 2021;149:111311. <https://doi.org/10.1016/j.rser.2021.111311>.
- [6] Fan L, Tu Z, Chan SH. Recent development of hydrogen and fuel cell technologies: a review. *Energy Rep Nov.* 2021;7:8421–46. <https://doi.org/10.1016/j.egy.2021.08.003>.
- [7] Tahan M-R. Recent advances in hydrogen compressors for use in large-scale renewable energy integration. *Int J Hydrogen Energy Oct.* 2022;47(83):35275–92. <https://doi.org/10.1016/j.ijhydene.2022.08.128>.

- [8] Lototskyy MV, Yartys VA, Pollet BG, Bowman RC. Metal hydride hydrogen compressors: a review. *Int J Hydrogen Energy* Apr. 2014;39(11):5818–51. <https://doi.org/10.1016/j.ijhydene.2014.01.158>.
- [9] Reilly JJ, Holtz A, Wiswall RH. A new laboratory gas circulation pump for intermediate pressures. *Rev Sci Instrum* Oct. 1971;42(10):1485–6. <https://doi.org/10.1063/1.1684913>.
- [10] Peng Z. Overview of hydrogen compression materials based on a three-stage metal hydride hydrogen compressor. *J Alloys Compd* Feb. 2022;895:161629. <https://doi.org/10.1016/j.jallcom.2021.162465>.
- [11] Lototskyy M, et al. Industrial-scale metal hydride hydrogen compressors developed at the South African Institute for Advanced Materials Chemistry. *Mater Today Proc* 2018;5(4):10514–23. <https://doi.org/10.1016/j.matpr.2017.12.383>.
- [12] Lototskyy MV, Yartys VA, Tarasov BP, Davids MW, Denys RV, Tai S. Modelling of metal hydride hydrogen compressors from thermodynamics of hydrogen – metal interactions viewpoint: Part I. Assessment of the performance of metal hydride materials. *Int J Hydrogen Energy* Jan. 2021;46(2):2330–8. <https://doi.org/10.1016/j.ijhydene.2020.10.090>.
- [13] Chen X, et al. Effect of Mn on the long-term cycling performance of AB5-type hydrogen storage alloy. *Int J Hydrogen Energy* Jun. 2021;46(42):21973–83. <https://doi.org/10.1016/j.ijhydene.2021.04.021>.
- [14] Li C-J, Wang F-R, Cheng W-H, Li W, Zhao W-T. The influence of high-rate quenching on the cycle stability and the structure of the AB5-type hydrogen storage alloys with different Co content. *J Alloys Compd* Feb. 2001;315(1–2): 218–23. [https://doi.org/10.1016/S0925-8388\(00\)01282-2](https://doi.org/10.1016/S0925-8388(00)01282-2).
- [15] Dematteis EM, Berti N, Cuevas F, Laroche M, Baricco M. Substitutional effects in TiFe for hydrogen storage: a comprehensive review. *Mater. Adv.* 2021;2(8): 2524–60. <https://doi.org/10.1039/D1MA00101A>.
- [16] Sujjan GK, Pan Z, Li H, Liang D, Alam N. An overview on TiFe intermetallic for solid-state hydrogen storage: microstructure, hydrogenation and fabrication processes. *Crit Rev Solid State Mater Sci Sep.* 2020;45(5):410–27. <https://doi.org/10.1080/10408436.2019.1652143>.
- [17] Hang Z, Xiao X, Li S, Ge H, Chen C, Chen L. Influence of heat treatment on the microstructure and hydrogen storage properties of Ti10V77Cr6Fe6Zr alloy. *J Alloys Compd* Jul. 2012;529:128–33. <https://doi.org/10.1016/j.jallcom.2012.03.044>.
- [18] Dehouche Z, Savard M, Laurencelle F, Goyette J. Ti–V–Mn based alloys for hydrogen compression system. *J Alloys Compd* Sep. 2005;400(1–2):276–80. <https://doi.org/10.1016/j.jallcom.2005.04.007>.
- [19] Yartys VA, Lototskyy MV. Laves type intermetallic compounds as hydrogen storage materials: a review. *J Alloys Compd* Sep. 2022;916:165219. <https://doi.org/10.1016/j.jallcom.2022.165219>.
- [20] Vanhanen J. Combined hydrogen compressing and heat transforming through metal hydrides. *Int J Hydrogen Energy* May 1999;24(5):441–8. [https://doi.org/10.1016/S0360-3199\(98\)00095-0](https://doi.org/10.1016/S0360-3199(98)00095-0).
- [21] Corgnale C, Sulic M. High pressure thermal hydrogen compression employing Ti_{1.1}CrMn metal hydride material. *J Phys Energy* Jan. 2020;2(1):014003. <https://doi.org/10.1088/2515-7655/ab47b0>.
- [22] Wang X, Chen R, Zhang Y, Chen C, Wang Q. Hydrogen storage alloys for high-pressure suprapure hydrogen compressor. *J Alloys Compd* Aug. 2006;420(1–2): 322–5. <https://doi.org/10.1016/j.jallcom.2005.11.001>.
- [23] Li Q, et al. Optimization of Ti–Zr–Cr–Fe alloys for 45 MPa metal hydride hydrogen compressors using orthogonal analysis. *J Alloys Compd* Dec. 2021;889:161629. <https://doi.org/10.1016/j.jallcom.2021.161629>.
- [24] Li H, Wang X, Dong Z, Xu L, Chen C. A study on 70MPa metal hydride hydrogen compressor. *J Alloys Compd* Jul. 2010;502(2):503–7. <https://doi.org/10.1016/j.jallcom.2010.04.206>.
- [25] Guo X, et al. Laves phase hydrogen storage alloys for super-high-pressure metal hydride hydrogen compressors. *Rare Met Jun.* 2011;30(3):227–31. <https://doi.org/10.1007/s12598-011-0373-7>.
- [26] Peng Z, et al. Ti–Cr–Mn–Fe-based alloys optimized by orthogonal experiment for 85 MPa hydrogen compression materials. *J Alloys Compd* Jan. 2022;891:161791. <https://doi.org/10.1016/j.jallcom.2021.161791>.
- [27] Charbonnier V, Enoki H, Asano K, Kim H, Sakaki K. Tuning the hydrogenation properties of Ti1+Cr2-Mn laves phase compounds for high pressure metal-hydride compressors. *Int J Hydrogen Energy* Oct. 2021;46(73):36369–80. <https://doi.org/10.1016/j.ijhydene.2021.08.143>.
- [28] Lemmon EW, Huber ML, Leachman JW. Revised standardized equation for hydrogen gas densities for fuel consumption applications. *J. Res. Natl. Inst. Stand. Technol. Nov.* 2008;113(6):341. <https://doi.org/10.6028/jres.113.028>.
- [29] Kandavel M, Bhat VV, Rougier A, Aymard L, Nazri G-A, Tarascon J-M. Improvement of hydrogen storage properties of the AB2 Laves phase alloys for automotive application. *Int J Hydrogen Energy* Jul. 2008;33(14):3754–61. <https://doi.org/10.1016/j.ijhydene.2008.04.042>.